IEEE Access
Multidisciplinary | Rapid Review | Open Access Journal

Received March 4, 2022, accepted March 12, 2022, date of publication March 15, 2022, date of current version March 22, 2022.

Digital Object Identifier 10.1109/ACCESS.2022.3159682

An Alternative Encoding of the Golden Code and Its Low Complexity Detection

HONGJUN XU, (Member, IEEE), AND NARUSHAN PILLAY
School of Engineering, University of KwaZulu-Natal, Durban 4041, South Africa
Corresponding author: Narushan Pillay (pillayn@ukzn.ac.za)

ABSTRACT The Golden code is a full-rate full-diversity (FRFD) space-time block code. The encoder of the Golden code takes four complex symbols and generates two pairs of Golden codewords. The encoding of each Golden codeword can be regarded as superposition coding with ''complex'' power allocation. In this paper, we propose an alternative encoding of the Golden code which can be regarded as superposition coding with ''real'' power allocation. The Golden code with ''complex'' power allocation or ''real'' power allocation is hereinafter referred to as the C-Golden code or R-Golden code, respectively. The R-Golden code also preserves the FRFD property. The R-Golden code can be easily implemented in passband modulation using in-phase and quadrature components compared to the C-Golden code. An equivalent received signal model of the R-Golden code system is constructed, then used to derive a closed-form on the lower bound of the average bit error probability. We further propose a low complexity detection scheme, the fast essentially maximum-likelihood detection with adaptive signal detection subset (FE-ML-ASDS) for the R-Golden code. Both simulation and theoretical results show that both the C-Golden code and the R-Golden code achieve the same error performance. Compared to the fast essentially ML detection with signal detection subset (FE-ML-SDS), at high signal-to-noise ratios, the proposed FE-ML-ASDS further reduces detection complexity by at least 68% for the 16QAM or 64QAM R-Golden code with three receive antennas.

INDEX TERMS C-Golden code, FE-ML-ASDS, FE-ML-SDS, Golden code, Golden codeword, maximum-likelihood detection, R-Golden code, superposition coding.

I. INTRODUCTION

For real-time applications in the next-generation of wireless communication systems, it is necessary to have high data transmission rate, good wireless link reliability and low complexity detection schemes. Multiplexing is a technique which can be used to increase data transmission rate, while diversity is an approach to improve link reliability. Multiple-input multiple-output (MIMO) techniques are able to offer either multiplexing gain and/or diversity order. But not all MIMO schemes simultaneously provide multiplexing gain and diversity order. There is a trade-off between multiplexing gain and diversity order in MIMO systems [1]. The trade-off between multiplexing gain and diversity order depends on the encoding scheme employed in the MIMO system.

For example, the Alamouti scheme [2], space-time labelling diversity (STLD) [3], and Golden code [4] are all space-time block codes (STBCs), which are all MIMO systems with two transmit antennas. In the above three STBC schemes, the Alamouti scheme is a full-diversity half-rate STBC code with linear maximum-likelihood (ML) detection, the STLD scheme is a labelling and full-diversity half-rate STBC code with $\mathcal{O}(M^2)$ detection complexity for ML detection, and the Golden code is a full-rate full-diversity (FRFD) STBC with $\mathcal{O}(M^4)$ detection complexity for ML detection, where M is the modulation order and the code rate is defined as the number of transmitted symbols per antenna use per transmission time slot.

Amongst the above three STBCs with two transmit antennas, Alamouti STBC has been used in modern wireless technologies like Wireless Fidelity (Wi-Fi) IEEE 802.11n [5] and IEEE 802.11ah low power Wi-Fi [6]. However, the Golden code is a competitor of the Alamouti STBC because the Golden code achieves both spatial multiplexing gains and full diversity order. The Golden code has already been incorporated in the IEEE 802.16 (WiMAX) standard [7]. In this paper, we focus on the Golden code with low complexity detection. Very recently, the component-interleaved Golden

The associate editor coordinating the review of this manuscript and approving it for publication was Wei Feng.

code (CI-Golden code) and the multiple complex symbol Golden code (MCS-Golden code) were proposed in [8] and [9]. Both the CI-Golden code and the MCS-Golden code are also full-rate STBC codes. Compared to the Golden code, both the CI-Golden code and the MCS-Golden code achieve higher diversity order and further improve error performance.

The encoder of the Golden code takes four complex symbols and generates four Golden codewords. Let $j = \sqrt{-1}$ be a complex number. There are four parameters in the four Golden codewords: $\alpha = 1 + j\bar{\theta}$, $\bar{\alpha} = 1 + j\theta$, $\theta = \frac{1+\sqrt{5}}{2}$ and $\bar{\theta} = 1 - \theta$. One of the four Golden codewords is $x_s = \frac{1}{\sqrt{5}}\alpha(x_1 + x_2\theta)$. Let $\alpha_1 = \frac{1}{\sqrt{5}}\alpha$, $\alpha_2 = \frac{1}{\sqrt{5}}\alpha\theta$. The Golden codeword is rewritten as $x_s = \alpha_1 x_1 + \alpha_2 x_2$. Borrowing the concept of the superposition coding in the downlink nonorthogonal multiple access (DL-NOMA) system, the encoding of the Golden code in the form of $x_s = \alpha_1 x_1 + \alpha_2 x_2$ can be regarded as superposition coding with "complex" power allocation. This is because $|\alpha_1|^2 + |\alpha_2|^2 = 1$, and both α_1 and α_2 are complex, not real.

Let $\alpha = 1 + j\bar{\theta} = |\alpha|e^{j\varphi}$. Motivated by real power allocation of superposition coding in DL-NOMA system, we rotate α by an angle $-\varphi$, and then we have $e^{-j\varphi}\alpha = |\alpha|$.

Similarly, we rotate $\frac{1}{\sqrt{5}}\alpha(x_1 + x_2\theta)$ by an angle $-\varphi$ then the encoding $\frac{1}{\sqrt{5}}\alpha(x_1 + x_2\theta)$ becomes $e^{-j\varphi}\frac{1}{\sqrt{5}}\alpha(x_1 + x_2\theta) = \beta_1(x_1 + x_2\theta) = \beta_1 x_1 + \beta_2 x_2$, where $\beta_1 = \frac{1}{\sqrt{5}}|\alpha|$, $\beta_2 = \frac{1}{\sqrt{5}}|\alpha|\theta$. The alternative encoding $\beta_1 x_1 + \beta_2 x_2$ can be regarded as superposition coding with "real" power allocation because $|\beta_1|^2 + |\beta_2|^2 = 1$, and both β_1 and β_2 are real, not complex. Similarly other Golden codewords can also be rotated until superposition coding with "real" power allocation is achieved. For convenience of discussion, the Golden code with "complex" power allocation and the Golden code with "real" power allocation are hereinafter referred as C-Golden code and R-Golden code, respectively. Since the average transmit signal power of $\beta_1 x_1 + \beta_2 x_2$ in the R-Golden code is the same as $\frac{1}{\sqrt{5}}\alpha(x_1 + x_2\theta)$ in the C-Golden code, the error performance of the R-Golden code system is the same as the C-Golden code system. In Eqs. (3) or (4) of [10], the variances of the equivalent channel models of error performance bound A, also explained that only the amplitudes, not the phases affect the error performance of the proposed system.

In the C-Golden code, one of the Golden codewords is rewritten as $x_s = \alpha_1 x_1 + \alpha_2 x_2$. Let $\alpha_i = \alpha_i^I + j\alpha_i^Q$, $i \in [1:2]$, $x_k = x_k^I + jx_k^Q$, $k \in [1:2]$, and $x_s = \alpha_1 x_1 + \alpha_2 x_2 = x_s^I + jx_s^Q$. Then we have:

$$x_s^I = \alpha_1^I x_1^I + \alpha_2^I x_2^I - \alpha_1^Q x_1^Q - \alpha_2^Q x_2^Q, \quad (1.1)$$
$$x_s^Q = \alpha_1^I x_1^Q + \alpha_2^I x_2^Q - \alpha_1^Q x_1^I - \alpha_2^Q x_2^I. \quad (1.2)$$

If we implement the baseband model $x_s = x_s^I + jx_s^Q$ in passband in terms of $y_s = x_s^I \cos(2\pi f_c t) + x_s^Q \sin(2\pi f_c t)$, where f_c is the carrier frequency, we have to implement $\alpha_1^I x_1^I + \alpha_2^I x_2^I - \alpha_1^Q x_1^Q - \alpha_2^Q x_2^Q$ for x_s^I and $\alpha_1^I x_1^Q + \alpha_2^I x_2^Q - \alpha_1^Q x_1^I - \alpha_2^Q x_2^I$ for x_s^Q.

Similarly, in the R-Golden code one of the Golden codewords is $\beta_1 x_1 + \beta_2 x_2$. Let $\tilde{x}_s = \beta_1 x_1 + \beta_2 x_2$. Then we further have $\tilde{x}_s = \tilde{x}_s^I + j\tilde{x}_s^Q$, where $\tilde{x}_s^I = \beta_1 x_1^I + \beta_2 x_2^I$ and $\tilde{x}_s^Q = \beta_1 x_1^Q + \beta_2 x_2^Q$. Compared to implementing $\alpha_1^I x_1^I + \alpha_2^I x_2^I - \alpha_1^Q x_1^Q - \alpha_2^Q x_2^Q$ for x_s^I and $\alpha_1^I x_1^Q + \alpha_2^I x_2^Q - \alpha_1^Q x_1^I - \alpha_2^Q x_2^I$ for x_s^Q in the C-Golden code, we only need to implement $\beta_1 x_1^I + \beta_2 x_2^I$ for $\tilde{x}_s^I$ and $\beta_1 x_1^Q + \beta_2 x_2^Q$ for $\tilde{x}_s^Q$, which is easily implemented in passband in terms of $y_s = \tilde{x}_s^I \cos(2\pi f_c t) + \tilde{x}_s^Q \sin(2\pi f_c t)$. In this paper, this is the key motivation to propose an alternative encoding of the Golden code.

The detection complexity of the optimal ML detection for the R-Golden code is extremely high, which is proportional to $\mathcal{O}(M^4)$. Thus a low complexity detection algorithm is also important to the applications of the R-Golden code. Based on the structure of the R-Golden code, all detection algorithms for the C-Golden code can be applied to detect the R-Golden code. Reduced complexity detection algorithms for the Golden code have been recently surveyed in [10]. Two new reduced complexity detection algorithms have also been proposed in [10]. These two detection algorithms are the fast essentially ML with signal detection subset (FE-ML-SDS) and the sphere decoding with signal detection subset (SD-SDS). The detection complexity of the FE-ML-SDS is $\mathcal{O}(2 \times {M_1}^2), M_1 \leq M$, which is much smaller than the ML detection complexity $\mathcal{O}(M^4)$. The average cardinality of the signal set used in SD-SDS is reduced from M^2 to ${M_1}^2$ for M-ary quadrature amplitude modulation (MQAM). The detection complexity of the SD-SDS is also greatly reduced compared to the conventional sphere decoding. Very recently, the sphere decoding with sorted signal detection subset (SD-SSDS) has been proposed in [9]. The detection complexity of the SD-SSDS is even smaller than the SD-SDS. In this paper, we only focus on the FE-ML based low complexity detections of the R-Golden code.

The threshold based signal detection (TSD) has been proposed to detect the transmitted symbols in the superposition coded signal for specific power allocation in the DL-NOMA system [11]. The TSD is modified to detect the superposition coded signal with non-specific power allocation. In the R-Golden code, x_1 and x_2 can be also estimated using the modified TSD. This is an important advantage compared to the C-Golden code. We will exploit this advantage in the FE-ML-SDS to further reduce detection complexity.

Given two complex symbols, the FE-ML-SDS algorithm decomposes the ML detection of four complex symbols into two ML detections of the remaining two complex symbols. These two given complex symbols belong to the predefined signal detection subsets. The FE-ML-SDS algorithm implemented two decompositions using the predefined signal detection subsets. In order to further reduce detection

complexity, in this paper, the FE-ML with adaptive signal detection subset (FE-ML-ASDS) is proposed. The FE-ML-ASDS is achieved by aid of the TSD.

Based on the above, the main contributions of this paper are summarized as:

• The alternative encoding of the Golden code is proposed in this paper. The alternative encoding of the Golden code is treated as superposition coding with "real" power allocation, which is named as R-Golden code. The R-Golden code is also an FRFD STBC. Compared to the C-Golden code, the R-Golden code is easily implemented in passband in terms of $y_s = x_s^I \cos(2\pi f_c t) + x_s^Q \sin(2\pi f_c t)$.

• The FE-ML-ASDS is also proposed in this paper. Compared to the FE-ML-SDS, the FE-ML-ASDS can further reduce detection complexity for the R-Golden code.

The remainder of the paper is organized as follows: In Section II, the system model, which includes the Golden codeword, the R-Golden codeword and the R-Golden code system, is presented. In Section III, we present the signal constellation of the R-Golden codewords and the TSD for the R-Golden codewords. The lower bound on the average bit error probability (ABEP) for the R-Golden code system is derived in Section IV. Different detection schemes, which includes QR decomposition based signal detection, fast essentially ML detection, FE-ML-SDS and the proposed FE-ML-ASDS, are described in Section V. In Section VI, the simulation results are demonstrated. Finally, the paper[1] is concluded in Section VII.

II. SYSTEM MODEL

The key component of the R-Golden code is the encoding of the Golden code. In this section, we firstly present the encoding of the C-Golden code, then describe the proposed alternative encoding of the Golden code, and finally present the R-Golden code system.

A. THE ENCODING OF THE C-GOLDEN CODE

The encoder of the C-Golden code takes four complex input symbols and outputs four super-symbols, which are regarded as Golden codewords in this paper. Suppose that information bits are grouped into four bit streams, $\boldsymbol{b}_i = [b_{i,1}\ b_{i,2}\ \cdots\ b_{i,m}]$, $i \in [1:4]$, $m = \log_2 M$, where M is the modulation order. Each bit stream $\boldsymbol{b}_i$ is then mapped onto a constellation point x_i of squared MQAM, $x_i \in \vec{\Omega}_M$, where $\vec{\Omega}_M$ is the signal set of MQAM signals. The C-Golden code transmission matrix is given by [2]:

$$\boldsymbol{X}^c = [\boldsymbol{X}_1^c \quad \boldsymbol{X}_2^c] = \begin{bmatrix} x_{11}^c & x_{21}^c \\ x_{12}^c & x_{22}^c \end{bmatrix}, \tag{2}$$

where x_{ik}^c, $i, k \in [1:2]$ are expressed as:

$$x_{11}^c = \frac{1}{\sqrt{5}}\alpha(x_1 + x_2\theta), \tag{3.1}$$
$$x_{12}^c = \frac{1}{\sqrt{5}}\alpha(x_3 + x_4\theta), \tag{3.2}$$
$$x_{21}^c = \frac{1}{\sqrt{5}}j\bar{\alpha}(x_3 + x_4\bar{\theta}), \tag{3.3}$$
$$x_{22}^c = \frac{1}{\sqrt{5}}\bar{\alpha}(x_1 + x_2\bar{\theta}). \tag{3.4}$$

In (3.1) to (3.4), $\theta = \frac{1+\sqrt{5}}{2}$, $\bar{\theta} = 1 - \theta$, $\alpha = 1 + j\bar{\theta}$ and $\bar{\alpha} = 1 + j\theta$. It is assumed that $E\{|x_i|^2\} = \varepsilon_\Omega$, $i \in [1:4]$. Let $x_{11}^c \in \vec{\Omega}_C$, where $\vec{\Omega}_C$ is the signal set of x_{11}^c. Appendix A in [10], shows that $x_{12}^c \in \vec{\Omega}_C$, $x_{21}^c \in \vec{\Omega}_C$ and $x_{22}^c \in \vec{\Omega}_C$. For convenience, in this paper, we regard x_{ik}^c, $i, k \in [1:2]$, as the C-Golden codewords.

B. THE ENCODING OF THE R-GOLDEN CODE

The encoder of the R-Golden code also takes four complex input symbols and produces four R-Golden codewords. The derivation of the four R-Golden codewords is based on the C-Golden codewords.

In (3.1) to (3.4), we let $\alpha = |\alpha|e^{j\varphi_1}$, $\bar{\alpha} = |\bar{\alpha}|e^{j\varphi_2}$ and $j\bar{\alpha} = |\bar{\alpha}|e^{j\varphi_3}$. We also let $\beta_1 = \frac{1}{\sqrt{5}}|\alpha|$, $\beta_2 = \frac{1}{\sqrt{5}}|\bar{\alpha}| = \frac{1}{\sqrt{5}}|\alpha|\theta$. It is noted that $(\beta_1)^2 + (\beta_2)^2 = 1$. It is also easy to derive that $\frac{1}{\sqrt{5}}|\bar{\alpha}|\bar{\theta} = \beta_2\bar{\theta} = -\beta_1$.

In order to implement superposition encoding with "real" power allocation, an alternative encoding of the Golden code is to rotate x_{11}^c and x_{12}^c by angle $-\varphi_1$, x_{21}^c by angle $-\varphi_3$ and x_{22}^c by angle $-\varphi_2$. Then we have:

$$x_{11}^s = e^{-j\varphi_1}x_{11}^c = \beta_1 x_1 + \beta_2 x_2, \tag{4.1}$$
$$x_{12}^s = e^{-j\varphi_1}x_{12}^c = \beta_1 x_3 + \beta_2 x_4, \tag{4.2}$$
$$x_{21}^s = e^{-j\varphi_3}x_{21}^c = \beta_2 x_3 - \beta_1 x_4, \tag{4.3}$$
$$x_{22}^s = e^{-j\varphi_2}x_{22}^c = \beta_2 x_1 - \beta_1 x_2, \tag{4.4}$$

where we used $\beta_2\bar{\theta} = -\beta_1$ in the derivation of (4.3) and (4.4).

Compared to the implementation of (3.1) to (3.2) in passband, in terms of $y = x^I \cos(2\pi f_c t) + x^Q \sin(2\pi f_c t)$ for $x = x^I + jx^Q$, the implementation of (4.1) to (4.4) is much simpler. This is the key advantage of the R-Golden code.

From (4.1) to (4.4), it is easily seen that there are two pairs of the R-Golden codewords, (x_{11}^s, x_{22}^s) and (x_{12}^s, x_{21}^s). Let $x_{11}^s \in \vec{\Omega}_S$, where $\vec{\Omega}_S$ is the signal set of x_{11}^s. We also have $x_{12}^s \in \vec{\Omega}_S$.

Given $x_i \in \vec{\Omega}_M$, we also have $-x_i \in \vec{\Omega}_M$. We further have $x_{22}^s \in \vec{\Omega}_S$ and $x_{21}^s \in \vec{\Omega}_S$.

Correspondingly, the R-Golden code transmission matrix is written as:

$$\boldsymbol{X}^s = [\boldsymbol{X}_1^s \quad \boldsymbol{X}_2^s] = \begin{bmatrix} x_{11}^s & x_{21}^s \\ x_{12}^s & x_{22}^s \end{bmatrix}. \tag{5}$$

In the R-Golden code system, x_1 and x_2 or x_3 and x_4 can be very easily detected using the TSD algorithm if x_{ik}^s,

[1]Notation: Bold letters are used to denote vectors and matrices. $[\cdot]^T$, $(\cdot)^H$, $|\cdot|$ and $\|\cdot\|_F$ represent the transpose, Hermitian, Euclidean and Frobenius norm operations, respectively. $\mathcal{D}(\cdot)$ is the constellation demodulator function. $(\cdot)^{-1}$ is the inverse. $E\{\cdot\}$ is the expectation operation. $j = \sqrt{-1}$ is a complex number. $\Re\{\cdot\}$ and $\Im\{\cdot\}$ are the real and imaginary parts, respectively, of a complex number.

$i, k \in [1:2]$ is known at the receiver. This is an important feature of the R-Golden code, which will be used to further reduce detection complexity of the FE-ML-ASDS. However, in the C-Golden code system, x_1 and x_2 or x_3 and x_4 may not be easily detected even if $x_{ik}^c, i, k \in [1:2]$ is known at the receiver.

C. THE R-GOLDEN CODE SYSTEM MODEL

Consider an R-Golden code system with $N_t = 2$ transmit antennas and N_r receive antennas, $N_r \geq N_t$ [10]. The received signal in time slot i, $i \in [1:2]$ is given by:

$$\boldsymbol{y}_i = \boldsymbol{H}_i \boldsymbol{X}_i^s + \boldsymbol{n}_i, \tag{6}$$

where $\boldsymbol{y}_i \in \mathbb{C}^{N_r \times 1}$ is the signal vector received in the i^{th}, $i \in [1:2]$ time slot. $\boldsymbol{H}_i = [\boldsymbol{h}_{i,1}\ \boldsymbol{h}_{i,2}]$ is the channel gain matrix corresponding to the i^{th} time slot with $\mathbb{C}^{N_r \times 1}$ column vectors $\boldsymbol{h}_{i,1}$ and $\boldsymbol{h}_{i,2}$. $\boldsymbol{n}_i \in \mathbb{C}^{N_r \times 1}$ is the additive white Gaussian noise (AWGN) vector for the i^{th} time slot.

The entries of $\boldsymbol{h}_{i,k}$ and $\boldsymbol{n}_i$ are independent and identically distributed (i.i.d.) complex Gaussian random variables (RVs) distributed as $CN(0,1)$ and $CN(0, \frac{2\varepsilon_\Omega}{\rho})$, respectively. $\frac{\rho}{2}$ is the average signal-to-noise ratio (SNR) at each receive antenna.

From (6), it is easily seen that each transmit antenna transmits two input symbols in two time slots. Hence, the R-Golden code also is a full-rate code. Further, it is also easily seen that each transmitted input symbol experiences two different fadings in two time slots. Therefore, the R-Golden code also achieves full-diversity order $2N_r$. So the R-Golden code also is an FRFD STBC.

III. SIGNAL CONSTELLATION OF THE R-GOLDEN CODEWORDS

Superposition coded signal constellation has been analyzed in [11]. In this section, we use the approach in [11] to analyze the signal constellation of the R-Golden codewords.

In the R-Golden code system, there are two pairs of four R-Golden codewords (x_{11}^s, x_{22}^s) and (x_{12}^s, x_{21}^s). However, in this section, we only analyze the signal constellation for one pair of R-Golden codeword (x_{11}^s, x_{22}^s). The approach can be used to analyze the signal constellation for another pair of R-Golden codeword.

Let $x_i = x_i^I + jx_i^Q, i \in [1:2]$. Then x_{11}^s and x_{22}^s in (4.1) and (4.4) are rewritten as:

$$x_{11}^s = x_{11}^I + jx_{11}^Q, \tag{7.1}$$
$$x_{22}^s = x_{22}^I + jx_{22}^Q, \tag{7.2}$$

where $x_{ii}^I = \Re\{x_{ii}^s\}$ and $x_{ii}^Q = \Im\{x_{ii}^s\}, i \in [1:2]$.

Let $p \in [I, Q]$. We further have $x_{11}^p = \beta_1 x_1^p + \beta_2 x_2^p$ and $x_{22}^p = \beta_1 x_1^p - \beta_2 x_2^p$. Both x_{11}^p and x_{22}^p show that the alternative encoding of the Golden code or superposition encoding can be decoupled into in-phase superposition encoding and quadrature superposition encoding. This is an important behaviour of the R-Golden code system. This important behaviour of R-Golden code can be applied into the FE-ML with ASDS to further reduce detection complexity. However, the C-Golden code does not have this important behaviour.

Let $p \in [I, Q]$ then $x_i^p \in \vec{\Omega}_K^p$, $\vec{\Omega}_K^p$ is the signal set of the amplitude shift keying (ASK) modulation with modulation order K. Since we only take into account squared MQAM in this paper, we have $K = \sqrt{M}$. The in-phase or quadrature components of x_{11}^p and x_{22}^p in (7.1) and (7.2) can be rewritten as:

$$x_{11}^p = \beta_1 x_1^p + \beta_2 x_2^p, \tag{8.1}$$
$$x_{22}^p = \beta_1 x_1^p - \beta_2 x_2^p, \tag{8.2}$$

where $x_{ii}^p \in \vec{\Omega}_S^p, i \in [1:2]$, $\vec{\Omega}_S^p$ is the signal set of x_{ii}^p with modulation order K^2.

Let $z_i^{k_i}$ be the signal value of x_i^p, where k_i is the signal index of x_i^p, $k_i \in [1:K]$. We also let $z_{s1}^{k_s}$ and $z_{s2}^{k_s}$ be the signal values of x_{11}^p and x_{22}^p, where k_s is the signal index of x_{11}^p and x_{22}^p and $k_s \in [1:K^2]$.

As discussed in [11], the superposition coding of (8.1) and (8.2) can be alternatively expressed as encoding functions f_1 and f_2. Given $x_i^p = z_i^{k_i}, i \in [1:2]$ then $x_{11}^p = z_{s1}^{k_s}$ and $x_{22}^p = z_{s2}^{k_s}$ are expressed as:

$$z_{s_1}^{k_s} = f_1\left(z_1^{k_1}, z_2^{k_2}\right), \tag{9.1}$$
$$z_{s_2}^{k_s} = f_2\left(z_1^{k_1}, z_2^{k_2}\right), \tag{9.2}$$

where $k_s = (k_1 - 1) \times K + k_2$. It is also noted that $z_{s1}^{k_s}, z_{s2}^{k_s} \in \vec{\Omega}_S^p$.

In the R-Golden code system, the encoding functions in (9.1) and (9.2) generate K^2 pairs of outputs $(z_{s1}^{k_s}, z_{s2}^{k_s})$ for $x_i^p = z_i^{k_i}, i \in [1:2]$. Thus the signal detection at the receiver can be regarded as two inverse functions f_1^{-1} and f_2^{-1}. Suppose that the x_{11}^p and x_{22}^p are estimated as $\hat{x}_{11}^p = \hat{z}_{s1}^{k_s}$ and $\hat{x}_{22}^p = \hat{z}_{s2}^{k_s}$ at the receiver then the estimation of $x_i^p, i \in [1:2]$ can be expressed as two inverse functions f_1^{-1} and f_2^{-1}, which are given by:

$$\left[\hat{x}_1^{1p} = z_1^{k_1}, \hat{x}_2^{1p} = z_2^{k_2}\right] = f_1^{-1}\left(\hat{z}_{s_1}^{k_s}\right), \tag{10.1}$$
$$\left[\hat{x}_1^{2p} = z_1^{k_1}, \hat{x}_2^{2p} = z_2^{k_2}\right] = f_2^{-1}\left(\hat{z}_{s_2}^{k_s}\right). \tag{10.2}$$

In (10.1) and (10.2), both $\hat{x}_1^{1p}$ and $\hat{x}_2^{1p}$ are estimated based on the received signal in time slot 1, while $\hat{x}_1^{2p}$ and $\hat{x}_2^{2p}$ are estimated based on the received signal in time slot 2. Suppose that the channel state information (CSI) is known at the receiver. Then $\hat{x}_i^{1p} = \hat{x}_i^{2p}, i \in [1:2]$ if noise is absent.

However, $\hat{x}_i^{1p}$ may be different from $\hat{x}_i^{2p}$ if there exists noise during transmission. The probability for $\hat{x}_i^{1p} = \hat{x}_i^{2p}$ increases as the SNR increases. At high SNR, the probability for $\hat{x}_i^{1p} = \hat{x}_i^{2p}$ is large. We will use $\hat{x}_i^{1p} = \hat{x}_i^{2p}$ to aid the FE-ML-ASDS to further reduce detection complexity.

Now we use an example to explain encoding functions (9.1) and (9.2) and detection functions (10.1) and (10.2). Suppose that the modulation in the R-Golden code system is 16QAM. Then we have $x_i^p \in \vec{\Omega}_4^p$, where $\vec{\Omega}_4^p = [-3, -1, 1, 3], i \in [1:2]$. We further have

TABLE 1. Alternative encoding outputs of golden code.

$z_{s_1}^1 = -4.129$ $z_{s_2}^1 = -0.975$	$z_{s_1}^2 = -2.428$ $z_{s_2}^2 = -2.026$	$z_{s_1}^3 = -0.727$ $z_{s_2}^3 = -3.078$	$z_{s_1}^4 = 0.975$ $z_{s_2}^4 = -4.129$
$z_{s_1}^5 = -3.078$ $z_{s_2}^5 = 0.727$	$z_{s_1}^6 = -1.376$ $z_{s_2}^6 = -0.325$	$z_{s_1}^7 = 0.325$ $z_{s_2}^7 = -1.376$	$z_{s_1}^8 = 2.026$ $z_{s_2}^8 = -2.428$
$z_{s_1}^9 = -2.026$ $z_{s_2}^9 = 2.428$	$z_{s_1}^{10} = -0.325$ $z_{s_2}^{10} = 1.376$	$z_{s_1}^{11} = 1.376$ $z_{s_2}^{11} = 0.325$	$z_{s_1}^{12} = 3.078$ $z_{s_2}^{12} = -0.727$
$z_{s_1}^{13} = -0.975$ $z_{s_2}^{13} = 4.129$	$z_{s_1}^{14} = 0.727$ $z_{s_2}^{14} = 3.078$	$z_{s_1}^{15} = 2.428$ $z_{s_2}^{15} = 2.026$	$z_{s_1}^{16} = 4.129$ $z_{s_2}^{16} = 0.975$

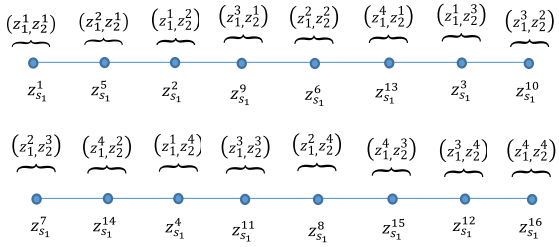

(a) Signal constellation of x_{11}^p

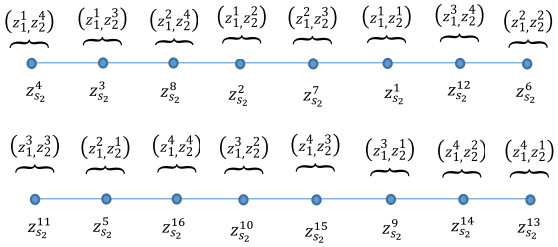

(b) Signal constellation of x_{22}^p

FIGURE 1. The signal constellation of x_{11}^p and x_{22}^p.

$z_i^1 = -3, z_i^2 = -1, z_i^3 = 1$ and $z_i^4 = 3$. Let $x_1^p = z_1^{k_1}, x_2^p = z_2^{k_2}, x_{11}^p = z_{s1}^{k_s}$ and $x_{22}^p = z_{s2}^{k_s}$ in (8.1) and (8.2), where $k_s = (k_1 - 1) \times 4 + k_2$. Then we have the alternative encoding $z_{s_1}^{k_s} = \beta_1 z_1^{k_1} + \beta_2 z_2^{k_2}$ and $z_{s_2}^{k_s} = \beta_1 z_1^{k_1} - \beta_2 z_2^{k_2}$. The alternative encoding outputs are tabulated in TABLE 1.

The above signal constellation of x_{11}^p and x_{22}^p is shown in FIGURE 1.

The TSD is proposed to detect the superposition coded signal with specific power allocation [11]. It is required the superposition coded signal $z_{s_i}^{k_s^2} > z_{s_i}^{k_s^1}$ for $k_s^2 > k_s^1$ given $z_i^{k_i^2} > z_i^{k_i^1}$ for $k_i^2 > k_i^1$. This is an important constraint to detect x_1^p and x_2^p using the TSD. From FIGURE 1 it is easy to know that the constellation in FIGURE 1 does not meet the constraint for the TSD algorithm. For example, FIGURE 1(a) shows $z_{s_1}^5 < z_{s_1}^2$ and FIGURE 1(b) shows $z_{s_2}^8 < z_{s_2}^2$.

In order to apply the TSD to detect both x_1^p and x_2^p, we perform an ascending sort for the superposition coded signal $z_{s_i}^{k_s}, k_s \in [1 : K^2]$, which is given by:

$$\left[\tilde{\boldsymbol{Z}}_{s_i} \ \boldsymbol{\Phi}_i\right] = argsort\left(\boldsymbol{Z}_{s_i}\right), \tag{11}$$

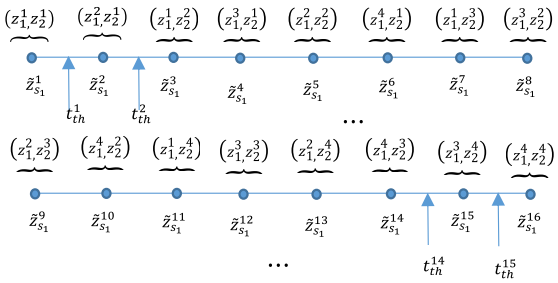

(a) Sorted signal constellation of x_{11}^p

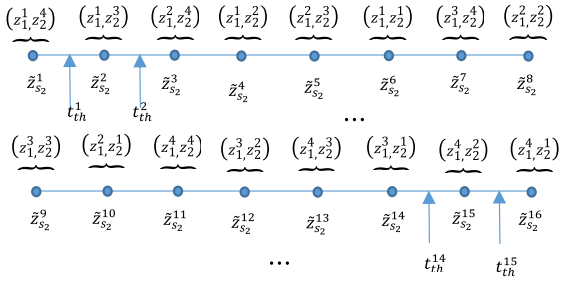

(b) Sorted signal constellation of x_{22}^p

FIGURE 2. The sorted signal constellation of x_{11}^p and x_{22}^p.

where $\boldsymbol{Z}_{s_i} = \left[z_{s_i}^1, \cdots, z_{s_i}^{K^2}\right]$ and $\tilde{\boldsymbol{Z}}_{s_i} = \left[\tilde{z}_{s_i}^{\Phi(l_1)}, \cdots, \tilde{z}_{s_i}^{\Phi(l_{K^2})}\right]$. Further $\left[\tilde{z}_{s_i}^{\Phi(l_1)}, \cdots, \tilde{z}_{s_i}^{\Phi(l_{K^2})}\right] = \left[\tilde{z}_{s_i}^1, \cdots, \tilde{z}_{s_i}^{K^2}\right]$. The $argsort\,(\cdot)$ operator arranges the K^2 elements in ascending order. $\boldsymbol{\Phi}_i$ is a vector of the index mapper, $\boldsymbol{\Phi}_i = \left[1, 2, \cdots, K^2\right] = \left[\Phi_i(l_1), \cdots, \Phi_i(l_{K^2})\right]$. Consequently a vector of the inverse index mapper is defined as $\boldsymbol{\Phi_i}^{-1} = \left[l_1, l_2, \cdots, l_{K^2}\right] = \left[\Phi_i(1)^{-1}, \cdots, \Phi_i(K^2)^{-1}\right]$.

In the above example, we have:

$$\boldsymbol{\Phi}_1^{-1} = \left[1, 5, 2, 9, 6, 13, 3, 10, 7, 14, 4, 11, 8, 15, 12, 16\right],$$
$$\boldsymbol{\Phi}_2^{-1} = \left[4, 3, 8, 2, 7, 1, 12, 6, 11, 5, 16, 10, 15, 9, 14, 13\right].$$

The signal constellation in terms of $\tilde{z}_{s_i}^{k_s}, k_s \in [1 : K^2]$ is shown in FIGURE 2.

We will apply the TSD in the new sequence $\tilde{\boldsymbol{Z}}_{s_i}$ to detect the transmitted x_1^p and x_2^p signals in Section V.

IV. ERROR PERFORMANCE ANALYSIS OF THE R-GOLDEN CODE

In R-Golden code system, four MQAM symbols are transmitted in two time slots using two transmit antennas. The received signal model for the R-Golden code is the same as the C-Golden code. The error performance of the C-Golden code has been analyzed in literature. Appendix B in [10] has proven that the bounded conditional pairwise error probability (PEP) for the C-Golden code at high SNR is equivalent to assume that only one input MQAM symbol is detected with errors, while the remaining three input MQAM symbols are detected correctly. The simulated error performance and the theoretical error performance derived in literature [10] validated that the above assumption works very well for $N_r \geq 3$

at high SNR for the C-Golden code. In the error performance analysis of the R-Golden code system, we also assume that one input MQAM symbol x_1, is detected with errors, while the remaining three input MQAM symbols x_i, $i \in [2:4]$, are detected correctly.

Then (6) can be simplified as:

$$\boldsymbol{y}_1 = \beta_1 \boldsymbol{h}_{1,1} x_1 + \boldsymbol{n}_1, \tag{12.1}$$
$$\boldsymbol{y}_2 = \beta_2 \boldsymbol{h}_{2,2} x_1 + \boldsymbol{n}_2. \tag{12.2}$$

Let $\tilde{\boldsymbol{h}}_{1,1} = \beta_1 \boldsymbol{h}_{1,1}$ and $\tilde{\boldsymbol{h}}_{2,2} = \beta_2 \boldsymbol{h}_{2,2}$. Then (12.1) and (12.2) may be rewritten as:

$$\boldsymbol{y}_1 = \tilde{\boldsymbol{h}}_{1,1} x_1 + \boldsymbol{n}_1, \tag{13.1}$$
$$\boldsymbol{y}_2 = \tilde{\boldsymbol{h}}_{2,2} x_1 + \boldsymbol{n}_2. \tag{13.2}$$

In (13.1) and (13.2), the entries of $\tilde{\boldsymbol{h}}_{1,1}$ and $\tilde{\boldsymbol{h}}_{2,2}$ are i.i.d. complex Gaussian RVs with distribution $CN(0,(\beta_1)^2)$ and $CN(0,(\beta_2)^2)$, respectively. Alternatively, the equivalent analysis model for error performance of the R-Golden code in (13.1) and (13.2), can be regarded as the transmission of x_1 over two non-identical fading channels with variance $(\beta_1)^2$ and $(\beta_2)^2$, respectively. The ABEP of the equivalent received signal model in (13.1) and (13.2) has been derived in Equ. (5) in [10], which is given by:

$$\begin{aligned} p_e \approx \frac{a}{c\log_2 M}\Bigg[&\frac{1}{2}\prod_{k=1}^{2}\left(\frac{2}{2+|\beta_k|^2 b\bar{\gamma}}\right)^{N_r} - \left(\frac{a}{2}\right) \\ &\times \prod_{k=1}^{2}\left(\frac{1}{1+|\beta_k|^2 b\bar{\gamma}}\right)^{N_r} \\ &+(1-a)\sum_{i=1}^{c-1}\prod_{k=1}^{2^n}\left(\frac{s_i}{s_i+|\beta_k|^2 b\bar{\gamma}}\right)^{N_r} \\ &+\sum_{i=c}^{2c-1}\prod_{k=1}^{2}\left(\frac{s_i}{s_i+|\beta_k|^2 b\bar{\gamma}}\right)^{N_r}\Bigg], \end{aligned} \tag{14}$$

where $c \geq 10$ is the number of partitioning intervals in this algorithm of numerical integration. $\bar{\gamma} = \frac{\rho}{2\varepsilon_\Omega}$, $a = 1 - \frac{1}{\sqrt{M}}$, $b = \frac{3}{M-1}$, and $s_i = 2\sin^2(\frac{i\pi}{4c})$.

Since only one input MQAM symbol is assumed to be detected with errors in the above derivation, (14) actually represents a lower bound on the ABEP of the R-Golden code system.

V. DETECTION SCHEMES FOR THE R-GOLDEN CODE SYSTEMS

In this section, we discuss the detection schemes for the R-Golden code system. We firstly present the QR decomposition based signal detection, then present the TSD, followed by the FE-ML-SDS, and finally describe the proposed FE-ML-ASDS.

A. QR DECOMPOSITION BASED SIGNAL DETECTION

Based on the complex QR decomposition, $\boldsymbol{H}_i$ in (6) is rewritten as:

$$\boldsymbol{H}_i = \boldsymbol{Q}_i \boldsymbol{R}_i, \tag{15}$$

where $\boldsymbol{Q}_i \in \mathbb{C}^{N_r \times N_r}$ is a unitary matrix, $\boldsymbol{R}_i \in \mathbb{C}^{N_r \times 2}$, $\boldsymbol{R}_i = \left[\boldsymbol{R}_{i1}\ \boldsymbol{R}_{i2}\right]^T$, where $\boldsymbol{R}_{i2}$ is a zero matrix with $(N_r - 2) \times 2$ dimension and $\boldsymbol{R}_{i1}$ is an upper-triangular matrix with 2×2 non-negative real diagonal elements, given by:

$$\boldsymbol{R}_{i1} = \begin{bmatrix} r_{i1}^{11} & r_{i1}^{12} \\ 0 & r_{i1}^{22} \end{bmatrix}. \tag{16}$$

Substituting $\boldsymbol{H}_i = \boldsymbol{Q}_i \boldsymbol{R}_i$ into $\boldsymbol{y}_i$, then (6) can be further written as:

$$\boldsymbol{y}_i = \boldsymbol{Q}_i \boldsymbol{R}_i \boldsymbol{X}_i^s + \boldsymbol{n}_i, \quad i \in [1:2]. \tag{17}$$

Now, multiplying both sides of (17) by $\boldsymbol{Q}_i^H$, we have:

$$\boldsymbol{z}_i = \boldsymbol{R}_i \boldsymbol{X}_i^s + \hat{\boldsymbol{n}}_i, \quad i \in [1:2], \tag{18}$$

where $\hat{\boldsymbol{n}}_i = \boldsymbol{Q}_i^H \boldsymbol{n}_i$ and $\boldsymbol{z}_i = \left[\boldsymbol{z}_i^1\ \boldsymbol{z}_i^2\right]^T = \boldsymbol{Q}_i^H \boldsymbol{y}_i$. $\boldsymbol{z}_i^1 = \left[z_i^{11}\ z_i^{12}\right]^T$ is a vector with 2×1 dimension and $\boldsymbol{z}_i^2$ is a vector with $(N_R - 2) \times 1$ dimension.

Based on $\boldsymbol{R}_i = \left[\boldsymbol{R}_{i1}\ \boldsymbol{R}_{i2}\right]^T$, ignoring the noise term in (18), we have:

$$\boldsymbol{z}_i^1 = \boldsymbol{R}_{i1} \boldsymbol{X}_i^s, \quad i \in [1:2]. \tag{19}$$

Based on the R-Golden transmission matrix in (5), the equivalent $u_{ij} = x_{ij}^s + n_{ij}, i, j \in [1:2]$ can be derived from (19), which are given by:

$$u_{12} = z_1^{12}/r_1^{22}, \tag{20.1}$$
$$u_{11} = \left(z_1^{11} - r_1^{12} u_{12}\right)/r_1^{11}, \tag{20.2}$$
$$u_{22} = z_2^{12}/r_2^{22}, \tag{20.3}$$
$$u_{21} = \left(z_2^{11} - r_2^{12} u_{22}\right)/r_2^{11}. \tag{20.4}$$

Let $\tilde{x}_i = x_i + \tilde{n}_i, i \in [1:4]$. Based on the superposition encoding in (4.1) to (4.4), $\tilde{x}_i$ can be further derived from u_{11} and u_{12} or u_{21} and u_{22}. The derived $\tilde{x}_i$ are given by:

$$\tilde{x}_1 = \beta_1 u_{11} + \beta_2 u_{22}, \tag{21.1}$$
$$\tilde{x}_2 = \beta_2 u_{11} - \beta_1 u_{22}, \tag{21.2}$$
$$\tilde{x}_3 = \beta_1 u_{12} + \beta_2 u_{21}, \tag{21.3}$$
$$\tilde{x}_2 = \beta_2 u_{12} - \beta_1 u_{21}. \tag{21.4}$$

Finally, the estimation of x_i is given by:

$$\hat{x}_i = \mathcal{D}(\tilde{x}_i), \quad i \in [1:4]. \tag{22}$$

The detection complexity of the QR decomposition based signal detection is very low. However, the error performance is worse compared o the ML detection. In the next subsection, we will present one of the low complexity detection schemes, the TSD.

B. THE THRESHOLD BASED SIGNAL DETECTION

In the previous subsection, the transmitted MQAM symbols x_i are estimated based on two time slot received signals. Alternatively, based on the received signal $\boldsymbol{y}_1$ or $\boldsymbol{y}_2$ in each time slot, the transmitted MQAM symbols x_i can be estimated by use of the TSD.

The thresholds play a key role in the TSD algorithm. Let t_{th}^k represent these thresholds in FIGURE 2 (a) and (b), where $k \in [1 : K^2 - 1]$. These thresholds t_{th}^k are easily derived as:

$$t_{th}^k = z_{s_i}^k + \frac{z_{s_i}^{k+1} - z_{s_i}^k}{2}, \tag{23}$$

The thresholds $t_{th}^k, k \in [1 : K^2 - 1]$ are also shown in FIGURES 2 (a) and (b).

Now we apply the TSD in [11] to the signal constellation in FIGURE 2 (a) and (b) to detect the transmitted signals. Since the TSD is not directly applied in FIGURE 1, we regard the signal detection scheme as a modified TSD.

As an example, let $x_1^p = -3$ and $x_2^p = 3$ based on the encoding of the R-Golden code, we have $x_{11}^p = \beta_1 x_1^p + \beta_2 x_2^p = z_{s_1}^4$ and $x_{22}^p = \beta_2 x_1^p - \beta_1 x_2^p = z_{s_2}^4$. It takes two time slots to transmit R-Golden codewords. x_{11}^p is transmitted at time slot one, while x_{22}^p is transmitted at time slot two. At the receiver, $u_{11}^p = x_{11}^p + n_{11}^p = z_{s_1}^4 + n_{11}^p$ and $u_{22}^p = x_{22}^p + n_{22}^p = z_{s_2}^4 + n_{22}^p$. Based on either u_{11}^p or u_{22}^p, the TSD can estimate the transmitted x_1^p and x_2^p. Let $\hat{x}_1^{t_1}$ and $\hat{x}_2^{t_1}$ be the estimations of the transmitted x_1^p and x_2^p based on u_{11}^p at time slot one and $\hat{x}_1^{t_2}$ and $\hat{x}_2^{t_2}$ be the estimations of the transmitted x_1^p and x_2^p based on u_{22}^p at time slot two.

Suppose $t_{th}^9 < u_{11}^p < t_{th}^{10}$ and $t_{th}^1 < u_{22}^p < t_{th}^2$ then the TSD estimates the transmitted x_1^p and x_2^p as $\hat{x}_1^{t_1} = -3$ and $\hat{x}_2^{t_1} = 3$ at time slot one and $\hat{x}_1^{t_2} = -3$ and $\hat{x}_2^{t_2} = 1$ at time slot two. From this example, it is seen that $\hat{x}_1^{t_1} = \hat{x}_1^{t_2}$, but $\hat{x}_2^{t_1} \neq \hat{x}_2^{t_2}$.

Similarly, applying the TSD on u_{12}^p and u_{21}^p the transmitted x_3^p and x_4^p can also be estimated.

In the above modified TSD, let $\hat{x}_i^{t_1}$ be the estimated MQAM symbols from u_{11} and u_{12} and $\hat{x}_i^{t_2}$ be the estimated MQAM symbols from u_{21} and u_{22}. It is easily seen that both $\hat{x}_i^{t_1}$ and $\hat{x}_i^{t_2}$ are based on one time slot received signal. It is also easily seen that $\hat{x}_i$ in (22) are based on two time slot received signals. The error performance of the above estimated $\hat{x}_i$ is better than $\hat{x}_i^{t_1}$ or $\hat{x}_i^{t_2}$. However, the error performance of the estimated $\hat{x}_i$ is still far from the optimal detection.

In the subsequent subsections, we will discuss another two low complexity detection schemes, the FE-ML-SDS and the proposed FE-ML-ASDS. The two low complexity detection schemes can achieve the optimal error performance.

C. FAST ESSENTIALLY ML DETECTION (FE-ML)

The FE-ML was proposed in [7], which reduces the detection complexity from $\mathcal{O}(M^4)$ to $\mathcal{O}(M^2)$. For convenient discussion of the FE-ML detection, we rewrite (6) as:

$$\boldsymbol{y}_1 = \boldsymbol{h}_{1,1} x_{11}^s + \boldsymbol{h}_{1,2} x_{12}^s + \boldsymbol{n}_1, \tag{24.1}$$
$$\boldsymbol{y}_2 = \boldsymbol{h}_{2,1} x_{21}^s + \boldsymbol{h}_{2,2} x_{22}^s + \boldsymbol{n}_2. \tag{24.2}$$

Substituting (4.1) to (4.4) into (24.1) and (24.2), we have:

$$\boldsymbol{Y} = \boldsymbol{H}_{13}\boldsymbol{X}_{13} + \boldsymbol{H}_{24}\boldsymbol{X}_{24} + \boldsymbol{N}, \tag{25}$$

where $\boldsymbol{Y} = \begin{bmatrix} \boldsymbol{y}_1 \ \boldsymbol{y}_2 \end{bmatrix}^T$, $\boldsymbol{H}_{13} = \begin{bmatrix} \beta_1 \boldsymbol{h}_{1,1} & \beta_1 \boldsymbol{h}_{1,2} \\ \beta_2 \boldsymbol{h}_{2,2} & \beta_2 \boldsymbol{h}_{2,1} \end{bmatrix}$, $\boldsymbol{H}_{24} = \begin{bmatrix} \beta_2 \boldsymbol{h}_{1,1} & \beta_2 \boldsymbol{h}_{1,2} \\ -\beta_1 \boldsymbol{h}_{2,2} & -\beta_1 \boldsymbol{h}_{2,1} \end{bmatrix}$, $\boldsymbol{X}_{13} = \begin{bmatrix} x_1 \ x_3 \end{bmatrix}^T$, $\boldsymbol{X}_{24} = \begin{bmatrix} x_2 \ x_4 \end{bmatrix}^T$ and $\boldsymbol{N} = \begin{bmatrix} \boldsymbol{n}_1 \ \boldsymbol{n}_2 \end{bmatrix}^T$.

Ignoring noise $\boldsymbol{N}$ in (25), the pair $\boldsymbol{X}_{13}$ of symbols can be estimated, given the pair $\boldsymbol{X}_{24}$ of symbols:

$$\tilde{\boldsymbol{X}}_{13} = (\boldsymbol{H}_{13}^H \boldsymbol{H}_{13})^{-1} \boldsymbol{H}_{13}^H (\boldsymbol{Y} - \boldsymbol{H}_{24}\boldsymbol{X}_{24}). \tag{26}$$

Alternatively, the pair $\boldsymbol{X}_{24}$ of symbols can be estimated, given the pair $\boldsymbol{X}_{13}$ of symbols:

$$\tilde{\boldsymbol{X}}_{24} = (\boldsymbol{H}_{24}^H \boldsymbol{H}_{24})^{-1} \boldsymbol{H}_{24}^H (\boldsymbol{Y} - \boldsymbol{H}_{13}\boldsymbol{X}_{13}). \tag{27}$$

The FE-ML detection is shown in Algorithm 1.

D. FAST ESSENTIALLY ML DETECTION WITH SIGNAL DETECTION SUBSET

The FE-ML detection algorithm searches the signal set $\vec{\Omega}_M$ to estimate $x_i, i \in [1 : 4]$. The detection complexity is proportional to $\mathcal{O}(M^2)$ for MQAM. In order to further reduce the detection complexity of the FE-ML, the FE-ML-SDS was proposed in [10]. The FE-ML-SDS only searches a part of the whole signal set $\vec{\Omega}_M$ to estimate $x_i, i \in [1 : 4]$.

The part of the whole signal set $\vec{\Omega}_M$ is referred to as SDS.

Definition 1: Given an i^{th} symbol $x = z_i$, an i^{th} SDS is defined as $\vec{\Omega}(z_i, \delta) = \{z_j, |z_j - z_i|^2 \leq \delta, j \in [1 : M]\}$.

The FE-ML-SDS algorithm firstly performs the coarse estimation of x_i given in (22) based on QR decomposition based detection, finds signal detection subset $\vec{\Omega}(\hat{x}_i, \delta)$ for each $\hat{x}_i$, replaces $\boldsymbol{\Omega}_M$ with $\vec{\Omega}(\hat{x}_i, \delta)$ in the FE-ML algorithm (Algorithm 1) and lastly conducts the final estimation of x_i.

As an example, we consider $x_i, i \in [1 : 4]$ being 16QAM symbols. Let $\delta = 4$. It is easily found that the average cardinality of $\vec{\Omega}(\hat{x}_i, \delta)$ is 4. The detection complexity is proportional to $\mathcal{O}(2 \times 4^2)$, which is much smaller than $\mathcal{O}(2 \times 16^2)$.

In general, the detection complexity is proportional to $\mathcal{O}(2 \times L_i^2)$, where L_i is the average cardinality of $\vec{\Omega}(\hat{x}_i, \delta)$. If the average cardinality of the signal detection subset is reduced, the overall detection complexity can be further reduced. In the next subsection, an adaptive signal detection subset is proposed to further reduce the average cardinality of the signal detection subset.

E. FAST ESSENTIALLY ML DETECTION WITH ADAPTIVE SIGNAL DETECTION SUBSET

For a given MQAM modulation, the average cardinality of the SDS in the FE-ML-SDS is constant. In order to further reduce the detection complexity for the FE-ML-SDS, the FE-ML-ASDS is proposed in this subsection. At high SNR the average cardinality of the adaptive SDS in the FE-ML-ASDS is reduced. The ASDS is achieved by the aid of $\hat{x}_i^{t_1}$ and $\hat{x}_i^{t_2}$, the detected MQAM symbols in the TSD, and the detected MQAM symbols $\hat{x}_i$ shown in (22) in the QR decomposition based signal detection, $i \in [1 : 4]$.

Let the estimation of x_i be z_i^k in QR decomposition based signal detection. That is $\hat{x}_i = z_i^k$. Then the SDS $\vec{\Omega}(\hat{x}_i, \delta)$

Algorithm 1 FE-ML Detection

Input: Received signal vectors $\boldsymbol{Y} = \left[\boldsymbol{y}_1\ \boldsymbol{y}_2\right]^T$, $\boldsymbol{H}_{13}, \boldsymbol{H}_{24}$ and $x_i \in \vec{\Omega}_M = \left[z_1 \cdots z_{K^2}\right]$.
Output: $\hat{x}_1, \hat{x}_2, \hat{x}_3, \hat{x}_4$.

Given $\boldsymbol{X}_{24}$ estimate $\boldsymbol{X}_{13}$;
$\boldsymbol{G}_1 = (\boldsymbol{H}_{13}^H \boldsymbol{H}_{13})^{-1} \boldsymbol{H}_{13}^H$;
for $k_2 \leftarrow 1$ **to** K^2 **do**
  for $k_4 \leftarrow 1$ **to** K^2 **do**
    $k \leftarrow (k_2 - 1) \times K^2 + k_4$;
    $x_2 \leftarrow z_{k_2}, x_4 \leftarrow z_{k_4}$;
    $\boldsymbol{X}_{24} = \left[x_2\ x_4\right]^T$;
    $\tilde{\boldsymbol{X}}_{13} = \boldsymbol{G}_1(\boldsymbol{Y} - \boldsymbol{H}_{24}\boldsymbol{X}_{24})$;
    $\hat{x}_1 = \mathcal{D}(\tilde{\boldsymbol{X}}_{13}(1)), \hat{x}_3 = \mathcal{D}(\tilde{\boldsymbol{X}}_{13}(2))$;
    $\hat{\boldsymbol{X}}^{13}(k,:) = \left[\hat{x}_1\ x_2\ \hat{x}_3\ x_4\right]^T$;
    $d^{13}(k) = \|\boldsymbol{Y} - (\boldsymbol{H}_{13}\hat{\boldsymbol{X}_{13}}(k) + \boldsymbol{H}_{24}\boldsymbol{X}_{24})\|_F^2$
  end for
end for
Given $\boldsymbol{X}_{13}$ estimate $\boldsymbol{X}_{24}$;
$\boldsymbol{G}_2 = (\boldsymbol{H}_{24}^H \boldsymbol{H}_{24})^{-1} \boldsymbol{H}_{24}^H$;
for $k_1 \leftarrow 1$ **to** K^2 **do**
  for $k_3 \leftarrow 1$ **to** K^2 **do**
    $k \leftarrow (k_1 - 1) \times K^2 + k_3$;
    $x_1 \leftarrow z_{k_1}, x_3 \leftarrow z_{k_3}$;
    $\boldsymbol{X}_{13} = \left[x_1\ x_3\right]^T$;
    $\tilde{\boldsymbol{X}}_{24} = \boldsymbol{G}_2(\boldsymbol{Y} - \boldsymbol{H}_{13}\boldsymbol{X}_{13})$;
    $\hat{x}_2 = \mathcal{D}(\tilde{\boldsymbol{X}}_{24}(1)), \hat{x}_4 = \mathcal{D}(\tilde{\boldsymbol{X}}_{24}(2))$;
    $\hat{\boldsymbol{X}}^{24}(k,:) = \left[x_1\ \hat{x}_2\ x_3\ \hat{x}_4\right]^T$;
    $d^{24}(k) = \|\boldsymbol{Y} - (\boldsymbol{H}_{13}\boldsymbol{X}_{13} + \boldsymbol{H}_{24}\hat{\boldsymbol{X}}_{24}(k))\|_F^2$
  end for
end for
$\left[d_m^{13}\ k_m^{13}\right] = \min_{k\in[1:K^4]}(d^{13}(k))$;
$\left[d_m^{24}\ k_m^{24}\right] = \min_{k\in[1:K^4]}(d^{24}(k))$;
$\hat{x}_1 = \hat{\boldsymbol{X}}^{13}(k_m^{13}, 1), \hat{x}_2 = \hat{\boldsymbol{X}}^{13}(k_m^{13}, 2), \hat{x}_3 = \hat{\boldsymbol{X}}^{13}(k_m^{13}, 3), \hat{x}_4 = \hat{\boldsymbol{X}}^{13}(k_m^{13}, 4)$;
if $d_{min}^{13} > d_{min}^{24}$ **then**
  $\hat{x}_1 = \hat{\boldsymbol{X}}^{24}(k_m^{24}, 1), \hat{x}_2 = \hat{\boldsymbol{X}}^{24}(k_m^{24}, 2), \hat{x}_3 = \hat{\boldsymbol{X}}^{24}(k_m^{24}, 3), \hat{x}_4 = \hat{\boldsymbol{X}}^{24}(k_m^{24}, 4)$;
end if

is found in Section D. Based on the Euclidean distances between $\hat{x}_i$ and the symbols in the SDS we sort all symbols in the SDS $\vec{\Omega}(\hat{x}_i, \delta)$ from the most probable transmitted to the least probable transmitted. The metric to estimate the possibilities of the transmitted symbols is given by:

$$m_i(k) = |\tilde{x}_i - \breve{x}_k|^2, \tag{28}$$

where $k \in [1 : L_i]$, and $\breve{x}_k \in \vec{\Omega}(\hat{x}_i, \delta)$, where L_i is the cardinality of $\vec{\Omega}(\hat{x}_i, \delta)$.

Let $\boldsymbol{m}_i = \left\{m_i(k), k \in [1 : L_i]\right\}, i \in [1 : 4]$. The most probable index estimation of x_i is obtained by evaluating:

$$\tilde{\boldsymbol{i}}_k = argsort\,(\boldsymbol{m}_i)\,, \tag{29}$$

TABLE 2. τ_k for the FE-ML-ASDS.

M	$N_r = 3$	$N_r = 4$
16	$\tau_1 = 1, \tau_2 = 3, \tau_3 = min(7, L_i)$	$\tau_1 = 1, \tau_2 = 2, \tau_3 = 3$
64	$\tau_1 = 1, \tau_2 = 3, \tau_3 = min(9, L_i)$	$\tau_1 = 1, \tau_2 = 2, \tau_3 = 3$

where the *argsort* $(\cdot)$ operator arranges the L_i elements from most probable to least probable. $\tilde{\boldsymbol{i}} = \left[\tilde{i}_1, \cdots, \tilde{i}_{L_i}\right]$.

Let τ_3, τ_2 and τ_1 be positive integers with $\tau_3 > \tau_2 > \tau_1$. If $\hat{x}_i^{t_1} = \hat{x}_i^{t_2} = z_i^k$ and $\hat{x}_i = z_i^k$, the probability of transmitting symbol $x_i = z_i^k$ is very large. In this case, we use small cardinality τ_1 to construct the signal detection subset for x_i.

If $\hat{x}_i^{t_1} = \hat{x}_i^{t_2} = z_i^k$, but $\hat{x}_i \neq z_i^k$. In this case, we use a little large cardinality τ_2 to construct the signal detection subset for x_i. The last case is $\hat{x}_i^{t_1} \neq \hat{x}_i^{t_2}$. In this case, we use large τ_3 to construct the signal detection subset for x_i. The implementation of ASDS is given in Algorithm 2.

Algorithm 2 Implementation of Adaptive Signal Detection Subset

Input: Estimation of transmitted x_i: $\hat{x}_i^{t_1}, \hat{x}_i^{t_2}$ and $\hat{x}_i, i \in [1 : 4]$, and three predetermined cadinalities: $\tau_l, l \in [1 : 3]$.
Output: $L_i, i \in [1 : 4]$

for $i \leftarrow 1$ **to** 4 **do**
  if $\hat{x}_i^{t_1} = \hat{x}_i^{t_2} = z_i^k$ and $\hat{x}_i = z_i^k$ **then**
    $L_i = \tau_1$;
  else if $\hat{x}_i^{t_1} = \hat{x}_i^{t_2} = z_i^k$ and $\hat{x}_i \neq z_i^k$ **then**
    $L_i = \tau_2$;
  else
    $L_i = \tau_3$;
  end if
end for

VI. SIMULATION RESULTS

In this section, we will present simulation results for the R-Golden code systems in frequency-flat Rayleigh fading with AWGN as described in Section II. It is assumed that the CSI is fully known at the receiver. As per the discussion in [10], the R-Golden code system is valid for $N_r \geq 2$.

However, in this section, we only consider $N_r > 2$ to enable comparison with the theoretical ABEP (14) derived in Section III. Based on TABLE 3 in [10], $\delta = 16$ and $\delta = 20$ are set for simulations of 16QAM and 64QAM Golden code with $N_r = 3$, respectively; and $\delta = 4$ is set for simulations of both 16QAM and 64QAM Golden code with $N_r = 4$.

Let L_i be the average cardinality of $\vec{\Omega}(\hat{x}_i, \delta)$. τ_k for the FE-ML-ASDS are tabulated in TABLE 2.

In the following two subsections, we firstly present the simulated detection complexity and then present the simulated bit error rate (BER).

A. DETECTION COMPLEXITY ANALYSIS

The detection complexity of the FE-ML-SDS has been analyzed in [10]. Similar to the discussion of detection complexity in [10], the metric of the detection complexity discussed

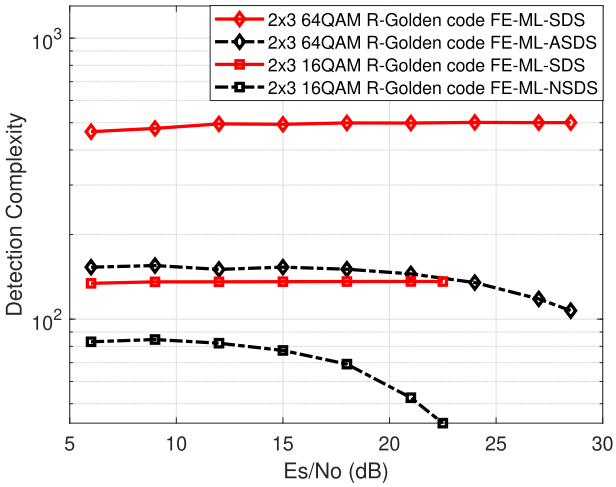

FIGURE 3. Detection Complexity versus normalized SNR for 16QAM and 64QAM R-Golden code with $N_r = 3$.

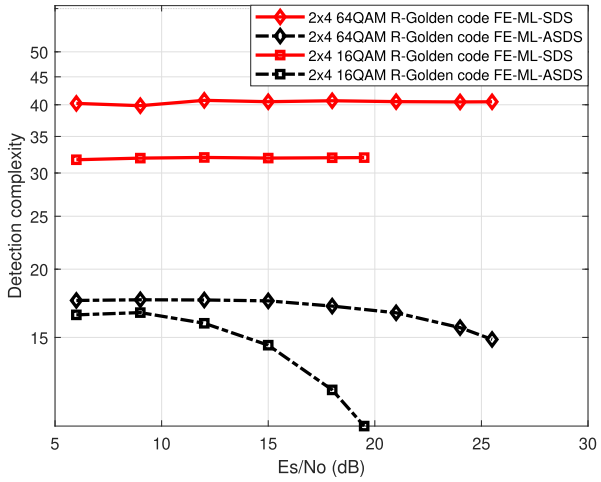

FIGURE 4. Detection Complexity versus normalized SNR for 16QAM and 64QAM R-Golden code with $N_r = 4$.

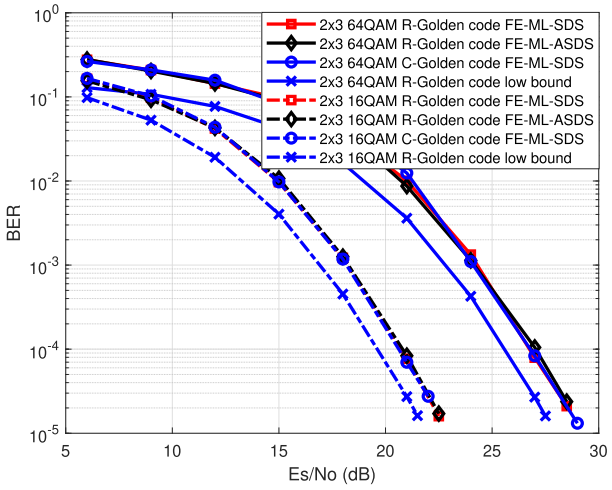

FIGURE 5. BER versus normalized SNR for 16QAM and 64QAM R-Golden code with $N_r = 3$.

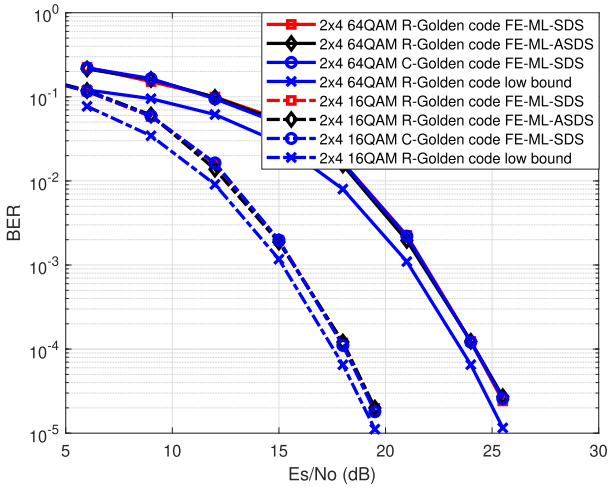

FIGURE 6. BER versus normalized SNR for 16QAM and 64QAM R-Golden code with $N_r = 4$.

in this paper, is in terms of the calculating (26) or (27) for detection of four MQAM symbols. The simulated detection complexities of the FE-ML-SDS and the FE-ML-ASDS for 16QAM and 64QAM R-Golden code with $N_r = 3$ and $N_r = 4$ are shown in FIGURES 3 and 4, respectively.

Let Com_{SDS} and Com_{ASDS} be the detection complexity of the FE-ML-SDS and the FE-ML-ASDS, respectively. Now we define the percentage of complexity reduction for the FE-ML-ASDS compared to the FE-ML-SDS as:

$$\beta = \frac{Com_{SDS} - Com_{ASDS}}{Com_{SDS}} \times 100. \tag{30}$$

From the simulated detection complexity in FIGURES 3 and 4 it is observed that:

1) The detection complexity of the FE-ML-SDS is almost constant because only one δ is used to construct symbol detection subsets.
2) The detection complexity of the proposed FE-ML-ASDS decreases as SNR increases. From Algorithm 2 it is seen that the lower end of the detection complexity of the FE-ML-ASDS is $(\tau_1)^2$.
3) For $N_r = 3$, $\beta = 78.6$ for 64QAM at 28.5 dB and $\beta = 68.7$ for 16QAM at 22.5 dB.
4) For $N_r = 4$, $\beta = 63.5$ for 64QAM at 25.5 dB and $\beta = 67.8$ for 16QAM at 19.5 dB.

B. BIT ERROR RATE ANALYSIS FOR R-GOLDEN CODE

In this paper, both the FE-ML-SDS and the FE-ML-ASDS are applied in the 16QAM and 64QAM R-Golden code with $N_r = 3$ and $N_r = 4$. Again, we set the simulation parameters for the R-Golden code according to TABLE 1 in this paper.

All BER simulation results of the two detection algorithms are shown in FIGURES 5 and 6. All theoretical results based on (14) are also shown in FIGURES 5 and 6. For comparison, we also simulated the 16QAM and 64QAM C-Golden codes.

The BER simulation results of the 16QAM and 64QAM C-Golden code are also shown in FIGURES 5 and 6.

From the results in FIGURES 5 and 6, it is observed that:

1) Both the C-Golden code and the R-Golden code achieve the same error performance. This is because the average transmit signal power of $\beta_1 x_1 + \beta_2 x_2$ in the R-Golden code is the same as $\frac{1}{\sqrt{5}}\alpha(x_1 + x_2\theta)$ in the C-Golden code.
2) As the number of receive antennas increases, the simulated BER draws closer to the theoretical bound.
3) For $N_r = 3$, the proposed FE-ML-ASDS detection algorithm achieves the same error performance of the FE-ML-SDS detection algorithm until a BER of 2×10^{-5}. However the detection complexity of the FE-ML-ASDS is much lower than the FE-ML-SDS at high SNR. This is because the proposed FE-ML-ASDS has a large probability to correctly estimate the transmitted symbols with small cardinality of the SDS at high SNR.

VII. CONCLUSION

In this paper, we proposed an alternative encoding of the Golden code. The alternative encoding of the Golden code is regarded as superposition coding with "real" power allocation. Compared to the C-Golden code, it is comparatively easy to implement the R-Golden code in passband modulation. The lower bound on the ABEP for the R-Golden code system was also derived. Furthermore, the FE-ML with adaptive SDS was proposed in this paper, to further reduce the detection complexity. Simulation and theoretical results validated that both the C-Golden code and the R-Golden code achieve the same error performance. For the R-Golden code system with $N_r = 3$, the detection complexity of the FE-ML-ASDS is at least 68 percent lower than the FE-ML-SDS at high SNR.

REFERENCES

[1] L. Zheng and D. N. C. Tse, "Diversity and multiplexing: A fundamental tradeoff in multiple-antenna channels," *IEEE Trans. Inf. Theory*, vol. 49, no. 5, pp. 1073–1096, May 2003.
[2] S. Alamouti, "A simple transmit diversity technique for wireless communications," *IEEE J. Sel. Areas Commun.*, vol. 16, no. 8, pp. 1451–1458, Oct. 1998.
[3] H. Xu, K. Govindasamy, and N. Pillay, "Uncoded space-time labeling diversity," *IEEE Commun. Lett.*, vol. 20, no. 8, pp. 1511–1514, Aug. 2016.
[4] J.-C. Belfiore, G. Rekaya, and E. Viterbo, "The golden code: A 2×2 full-rate space-time code with nonvanishing determinants," *IEEE Trans. Inf. Theory*, vol. 51, no. 4, pp. 1432–1436, Apr. 2005.
[5] F. Riera-Palou and G. Femenias, "Improving STBC performance in IEEE 802.11n using group-orthogonal frequency diversity," in *Proc. IEEE Wireless Commun. Netw. Conf. (WCNC)*, Las Vegas, NV, USA, Mar. 2008, pp. 193–198.
[6] *IEEE Standard for Information Technology—Telecommunications and Information Exchange Between Systems Local and Metropolitan Area Networks—Specific Requirements—Part 11: Wireless Local Area Network (LAN) Medium Access Control (MAC) and Physical Layer (PHY) Specifications—Amendment 2: Sub 1 GHz License Exempt Operation*, IEEE Standard 802.11ah-2016 (Amendment to IEEE Std 802.11-2016, as amended by IEEE Std 802.11ai-2016), 2017.
[7] S. Sirinaunpiboon, A. R. Calderbank, and S. D. Howard, "Fast essentially maximum likelihood decoding of the Golden code," *IEEE Trans. Inf. Theory*, vol. 57, no. 6, pp. 3537–3541, Jun. 2011.
[8] H. Xu and N. Pillay, "The component-interleaved golden code and its low-complexity detection," *IEEE Access*, vol. 8, pp. 59551–59558, 2020.
[9] H. Xu and N. Pillay, "The multiple complex symbol golden code," *IEEE Access*, vol. 8, pp. 103577–103584, 2020.
[10] H. Xu and N. Pillay, "Reduced complexity detection schemes for golden code systems," *IEEE Access*, vol. 7, pp. 139140–139149, 2019.
[11] H. Xu and N. Pillay, "Threshold based signal detection and the average symbol error probability for downlink NOMA systems with M-ary QAM," *IEEE Access*, vol. 8, pp. 156677–156685, 2020.

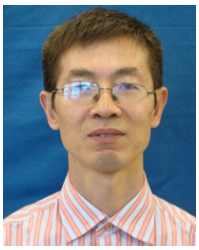

HONGJUN XU (Member, IEEE) received the B.Sc. degree from the Guilin University of Electronic Technology, China, in 1984, and the M.Sc. degree from the Institute of Telecontrol and Telemeasure, Shi Jian Zhuang, China, 1989, and the Ph.D. degree from the Beijing University of Aeronautics and Astronautics, Beijing, China, 1995. Currently, he is a Full Professor with the School of Engineering, University of KwaZulu-Natal, Howard College Campus. He was a Postdoctoral Researcher at the University of Natal and Inha University, from 1997 to 2000. He has published more than 50 journal articles. His research interests include digital and wireless communications and digital systems. He is also a National Research Foundation (NRF)-Rated Researcher in South Africa.

NARUSHAN PILLAY received the M.Sc.Eng. *(cum laude)* and Ph.D. degrees in wireless communications from the University of KwaZulu-Natal, Durban, South Africa, in 2008 and 2012, respectively. He has been with the University of KwaZulu-Natal, since 2009. Previously, he was at the Council of Scientific and Industrial Research (CSIR), Defence, Peace, Safety and Security (DPSS), South Africa. He has published several articles in well-known journals in his area of research. His research interests include physical wireless communications, including spectrum sensing for cognitive radio, and MIMO systems. He currently supervises several Ph.D. and M.Sc.Eng. degrees students. He is an National Research Foundation (NRF)-Rated Researcher in South Africa.